frontiers | Frontiers in Materials

TYPE Original Research
PUBLISHED 21 October 2022
DOI 10.3389/fmats.2022.1049304

OPEN ACCESS

EDITED BY
Lei Wang,
Xi'an University of Architecture and Technology, China

REVIEWED BY
Shengwen Tang,
Wuhan University, China
Mehmet Serkan Kirgiz,
Istanbul Sabahattin Zaim University, Turkey

*CORRESPONDENCE
Lijuan Zhang,
zhanglj0526@zzu.edu.cn

SPECIALTY SECTION
This article was submitted to Structural Materials, a section of the journal Frontiers in Materials

RECEIVED 20 September 2022
ACCEPTED 03 October 2022
PUBLISHED 21 October 2022

CITATION
Ding D, Zhang L, Zhao J, Li C and Wang Z (2022), Effects of air-entraining agent and polypropylene fiber on the mechanical properties, autogenous shrinkage, and fracture properties of fully recycled aggregate concrete. *Front. Mater.* 9:1049304. doi: 10.3389/fmats.2022.1049304

Effects of air-entraining agent and polypropylene fiber on the mechanical properties, autogenous shrinkage, and fracture properties of fully recycled aggregate concrete

Dong Ding, Lijuan Zhang*, Jun Zhao, Changbin Li and Zhi Wang

School of Mechanics and Safety Engineering, Zhengzhou University, Zhengzhou, China

The effects of air-entraining agent (AEA) and polypropylene fiber (PPF) on the autogenous shrinkage and fracture properties of fully recycled aggregate concrete (FRAC) are studied to obtain FRAC with low density, low autogenous shrinkage, and superior fracture properties. Six groups of FRAC with different AEA (0, 5%, 10%) and PPF (0, 1.2 kg/m^3) contents were prepared for test. The results illustrate that AEA can slightly reduce density but that it has an adverse effect on the strength and fracture properties of FRAC. The incorporation of PPFs can reduce the adverse effect of AEA on compressive strength and splitting tensile strength, but it will increase the adverse effect on fracture properties. Furthermore, the addition of PPFs alone will significantly reduce compressive strength and splitting tensile strength, whereas flexural strength and fracture properties are increased. The addition of AEA can improve the adverse effect of PPFs on compressive strength and splitting tensile strength, but flexural strength and fracture properties will decrease rather than increase. The addition of 10% AEA can greatly reduce autogenous shrinkage, and 5% AEA can reduce autogenous shrinkage at an early age. Incorporating PPFs can further reduce autogenous shrinkage. The study mainly examines the effects of AEA and PPF on the autogenous shrinkage of FRAC, and provides some new ideas for producing high-performance FRAC. At the same time, the cooperative effect of AEA and PPF on the properties of FRAC is also studied.

KEYWORDS

recycled aggregate concrete, air-entraining agent, polypropylene fiber, strength, autogenous shrinkage, fracture properties

1 Introduction

Concrete is a composite material widely used in the construction, electrical, mechanical, and chemical industries, which demands a large amount of natural gravel and river sand in the course of its pouring process. Roughly 32 billion to 50 billion tons of sand are used globally each year; the mining speed of sand and gravel, two non-renewable natural resources, far exceeds the pace of natural renewal (Bendixen et al., 2019). The excessive mining of river sand has lowered water tables and hastened river-bed scour, damaging bridges and embankments, thus causing a sequence of environmental, social, and economic problems (Torres et al., 2017). On the other hand, with rapid urbanization, a mass of construction and demolition (C&D) wastes are generated annually in the process of reconstruction and new construction. In China, 1.55–2.40 billion tons of C&D wastes are produced every year (Liu et al., 2020), causing environmental pollution and the waste of resources. Recycling C&D wastes is a significant step in the pursuit of global environmental sustainability (Anike et al., 2019; Yang et al., 2022). The treatment and application of C&D wastes are major problems in the development of urban construction. The application technology of recycled aggregate concrete (RAC) can not only reduce the mining of natural gravel and river sand but can also effectively consume C&D wastes (Deresa et al., 2020).

According to particle size, products derived from C&D wastes mainly include recycled coarse aggregate (RCA), recycled fine aggregate (RFA), and recycled powder (RP). Compared with natural coarse aggregate (NCA), RCA has lower density and higher water absorption due to the old cement mortar adhering to its surface (Shi et al., 2016). Moreover, the damage accumulation of C&D wastes in the process of recycling and crushing causes a large number of tiny cracks in RCA, resulting in its lower strength (Cakir, 2014). Because of the difference in the physical properties of RCA and NCA, the mechanical properties and durability of recycled aggregate concrete (RAC) are lower than natural aggregate concrete (NAC) (Guo et al., 2018). About 40% of products produced from C&D wastes are RFA and RP (Zhang et al., 2022) but RFA is generally considered a low-value product and is severely restricted in application to concrete manufacture because of its instability, high water absorption, and high quantity of old cement mortar (Evangelista and De Brito, 2014). In order to make full use of C&D waste, much research has investigated improving the properties of RAC through the mix design (Bidabadi et al., 2020) or incorporating reinforcing materials (Cantero et al., 2020). However, both of these increase cost, thus restricting RAC's large-scale engineering application.

Cracking can affect the overall performance of concrete and accelerate the corrosion of its steel reinforcement; this can be divided into non-load and load cracking. About 80% of non-load cracking is caused by concrete shrinkage. The autogenous shrinkage of concrete is defined as a reduction in volume which occurs without moisture exchange between the internal concrete and external air (Zhang et al., 2020), triggered by self-drying from the hydration reaction of cement (Hua et al., 1995; Tazawa and Miyazawa, 1995). Autogenous shrinkage usually occurs in the early stage of the hydration reaction of concrete. At this stage, the concrete's tensile strength is low, and may not be enough to withstand the stress generated by autogenous shrinkage, thus causing early cracking (Wang et al., 2022a). In high performance concrete (HPC), the effect of autogenous shrinkage is more significant, and the development of RAC is also trending towards high performance. Therefore, it is very important to study how to reduce the autogenous shrinkage of RAC. Fracture properties are the evaluation criteria of the resistance of concrete to the unstable development of initial cracking under load. Several studies indicate that, with an increase in the replacement rate of RCA, the fracture properties sharply reduce (Choubey et al., 2016).

Air-entraining agent (AEA) is often used in concrete manufacturing in cold regions, since pores exert a pivotal role in concrete structures against freeze–thaw action—pores act as a reserve of volume against water expansion when concrete freezes. AEA can introduce tiny air bubbles of up to 100 μm in size inside concrete (Chen et al., 2014). Therefore, structural standards in cold regions generally require the use of AEA in concrete manufacturing with the aim of assuring proper freeze–thaw strength. The correct application of AEA can provide adequate protection against internal cracking in concrete subjected to freeze–thaw action (Wu et al., 2020; Gonzalez et al., 2021). The addition of AEA can also reduce the density of concrete, enhance its workability (Ruan and Unluer, 2017), and improve its fire resistance (Khaliq and Waheed, 2017) and crack resistance (Wang et al., 2014).

Polypropylene fiber (PPF) is a milky-white, tasteless, odorless, non-toxic, economical, and lightweight material; it rarely corrodes in concrete and resists aggressive chemical erosion (Deng et al., 2020). Incorporating PPF into concrete can increase concrete's splitting tensile strength (Li et al., 2016), flexural strength (Cho et al., 2014), impact resistance (Md and Unnikrishnan, 2022), crack resistance (Wang et al., 2021), and ductility (Orouji et al., 2021). The addition of PPFs can also reduce its autogenous and total shrinkage (Saje et al., 2011) and improve fracture properties (Liang et al., 2021).

In this paper, both RCA and RFA were used to make FRAC. AEA and PPF were mixed into FRAC as the main experimental variables in the expectation that FRAC would obtain a light density and good crack resistance, and also meet the requirements of building structure engineering. This would provide a method for making high-performance FRAC. Fly ash and water-reducing agent were used to improve the pore structure and workability (Wang et al., 2022b). The mechanical properties, autogenous shrinkage, and fracture properties of

TABLE 1 Properties of aggregate.

	RCA	GB/T 25,177	NCA	RFA	GB/T 14,684	NFA
Apparent density (kg/m^3)	2734.8	>2450	2814	2594.7	>2500	2556.2
Water absorption (%)	2.56	<4.0	1.4	3.7	—	0.56
Crush index (%)	14.1	<12	8.8	—	—	—
Fineness modulus	—	—	—	3.15	2.3–3.2	2.67

FRAC were mainly tested; the double-K fracture model (Shilang and Reinhardt, 1999a; Shilang and Reinhardt, 1999b) was used to evaluate the fracture properties of FRAC.

2 Experimental programs

2.1 Materials

Grade 42.5 Portland cement, recycled coarse aggregate (RCA), recycled fine aggregate (RFA), polypropylene fiber (PPF), air-entraining agent (AEA), water-reducing agent (WRA), and fly ash were used in the test. The properties of RCA and RFA are shown in Table 1. China's national standards for first-grade recycled aggregate for construction and the properties of local natural aggregate are also included in Table 1 for reference. The RCA used in this experiment conforms to the stipulations in Chinese standard GB/T 25177-2010 (China National Standardization Administration Committee and General Administration of Quality Supervision Inspection and Quarantine of the People's Republic of China, 2010) and belongs to second-grade recycled coarse aggregate for construction. The RFA also conforms to the stipulations of Chinese standard GB/T 14684-2022 (Ahmed and Maalej, 2009; National Standardization Management Committee and State Administration of Market Supervision and Administration, 2022). The fineness modulus of RFA was 3.15, greater than 3 and less than 3.2, and is thus first-grade coarse sand. Compared to NCA in literature (Gao et al., 2017), RCA has higher water absorption, higher crush index, and lower apparent density; thus, its strength is worse and quality lighter. The apparent density of RFA is similar to that of NFA, but its water absorption is about six times higher. The specific surface area values of Portland cement and fly ash are 1.16 and 1.05 m^2/g, respectively. The length of polypropylene fiber was 9 mm and its density was 0.9 kg/m^3. The air-entraining agent was GYQ-3 high-efficiency air-entraining agent, and the water-reducing agent was a polycarboxylic acid water-reducing agent with a water-reducing rate of 27%.

The water/cement ratio was 0.53, the sand ratio 0.35, and mixes with fly ash accounted for 30% of the total cement weight. The content of air-entraining agent was selected as 0, 5%, and 10%, (the ratio of the weight of air-entraining agent to the weight of cement). The content of polypropylene fiber was 1.2 kg/m^3, equivalent to 0.13% volume rate. Detailed concrete composition is shown in Table 2. In the table, notation Y represents the content of air-entraining agent, notation P represents the content of polypropylene fiber; thus, Y5P1.2 represents a specimen with 5% air-entraining agent and 1.2 kg/m^3 polypropylene fibers.

The mixing process was as follows. Firstly, cement, fly ash, sand, and fiber were added in a concrete mixer and mixed for 2 min to ensure the fibers were well dispersed. Secondly, air-entraining agent, water-reducing agent, and half of the water were added to the mixer and stirred for 1 min to mix the materials into mortar, allowing the air-entraining agent and the water-reducing agent to fully react. Finally, the recycled coarse aggregate and the remaining water were added and mixed thoroughly for 1 min. After blending, the concrete was put into the mold and vibrated on the vibrating table for 60 s, before its surface was smoothed and put into a standard curing room with a 20°C temperature and 90% humidity.

2.2 Measurement methods

2.2.1 Mechanical properties

The 100 mm^3 cube specimens were used to test density, compressive strength, and splitting tensile strength. The compressive load was maintained at a loading speed of 0.5 MPa/s and the load-of-splitting tensile strength test was maintained at a loading speed of 0.02 MPa/s. The 100 mm × 100 mm × 400 mm prism specimens were used to test flexural strength by a four-point flexural test with a loading speed of 0.02 MPa/s. The mechanical properties testing equipment and the methods of specimens met the requirements of Chinese standard GB/T 50081-2019 (Ministry of Housing and Urban-Rural Development of the People's Republic of China and State Administration for Market Regulation, 2019).

2.2.2 Autogenous shrinkage properties

The autogenous shrinkage test was carried out with 100 mm × 100 mm × 515 mm prism specimens, using a non-contact concrete shrinkage tester, which met the

TABLE 2 Detailed composition/(kg/m^3).

Material	Y0P0	Y0P1.2	Y5P0	Y5P1.2	Y10P0	Y10P1.2
Water	205	205	205	205	205	205
Cement	273	273	273	273	273	273
Fly ash	117	117	117	117	117	117
Coarse aggregate	1,130	1,130	1,045	1,045	960	960
Fine aggregate	610	610	560	560	515	515
Air-entraining agent	0	0	13.65	13.65	27.3	27.3
Water-reducing agent	8.19	8.19	5.46	5.46	2.73	2.73
Polypropylene fiber	0	1.2	0	1.2	0	1.2
Weight	2235	2235	2200	2200	2070	2070

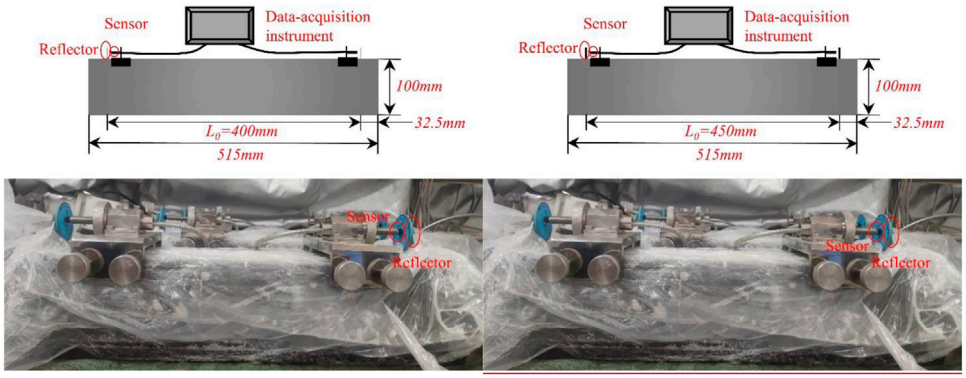

FIGURE 1
Non-contact concrete shrinkage tester.

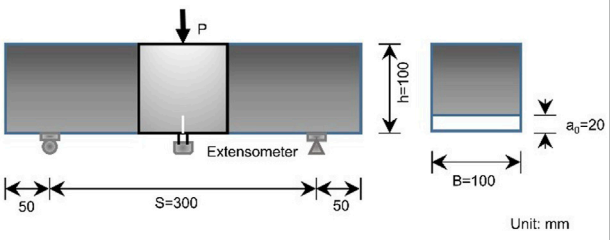

FIGURE 2
Size of specimen and crack.

requirements of Chinese standard GB/T 50082-2009 (Ministry of Housing and Urban-Rural Development of China and General Administration of Quality Supervision Inspection and Quarantine of the People 's Republic of China, 2009). Two reflectors were placed in the mold; the initial distance between them—L_0—was 450 mm. The reflector could move with the shrinkage of the concrete, and two sensors were used to measure the displacement of the reflectors. After the concrete was poured into the mold, the surface of the specimen was covered with PVC film to test the autogenous shrinkage of the concrete in an unconstrained state without moisture exchange. The autogenous shrinkage deformation of the specimen was recorded every hour, with a total of 28 days of data recorded. The diagram of the tester is shown in Figure 1.

2.2.3 Fracture properties

A three-point bending test was conducted with a notched prism specimen of 100 mm × 100 mm × 400 mm to investigate fracture properties. A prefabricated incision with a length of 20 mm was cut at the center line of the bottom of the prism to install a displacement extensometer to measure the crack-mouth opening displacement. The size of the specimen and crack are shown in Figure 2. A camera was used to record the occurrence and expansion of the crack.

TABLE 3 Mechanical properties' parameters of the tested specimens.

Specimen ID	Density (kg/m^3)	Compressive strength (MPa)	Splitting tensile strength (MPa)	Flexural strength (MPa)
Y0P0	2215	25.1	2.04	3.89
Y0P1.2	2253	21.8	1.29	4.14
Y5P0	2214	18.8	1.43	3.26
Y5P1.2	2204	17.1	1.20	3.12
Y10P0	2167	14.4	0.98	3.03
Y10P1.2	2165	14.1	1.14	2.81

FIGURE 3
(A) Splitting tensile failure section. **(B)** Flexural failure section.

3 Experimental results and discussion

The test results for density, compressive strength, splitting tensile strength, and flexural strength are listed in Table 3.

3.1 Failure phenomenon

As can be observed from Table 3, AEA and PPFs have little effect on the density of the specimen. In the three-point bending test, cracking generally emerges from the incision of the prism. As the load increases, cracks extend from bottom to top along the middle of the prism. Generally, after the prism reaches critical load, the main crack extends to about one-third of the upper part of the prism. The width of the crack was up to about 0.2 mm, with several small cracks next to the main crack. A similar phenomenon appears at the same position on the back of the other notched prisms.

The sections of FRAC after splitting tensile failure and flexural failure are shown in Figures 3A,B, respectively. As can be observed from Figure 3A, when the specimen experiences splitting tensile failure, most damage to RCA is obvious. This situation also appears in the flexural strength test. The phenomenon shows that the strength of RCA is low. The strength of FRAC is mainly controlled by the strength of RCA.

3.2 Mechanical properties

3.2.1 Compressive strength

According to the data in Table 3, the effects of the content of AEA and PPFs on the mechanical properties of FRAC can be represented in Figures 4, 5, respectively. As can be observed from the top of Figure 4, the compressive strength of the specimen decreases with the increase of AEA. As the content of AEA increases from 0 to 5%, the compressive strength of the specimen decreases by 25.1%. As the content of AEA is 10%, compared with specimens mixed with 0 and 5% AEA, the compressive strength is reduced by 42.6% and 23.4%. When mixing PPF and AEA in the FRAC at the same time, the content of AEA increases from 0 to 5% and the compressive strength of the specimen is reduced at a rate of 21.6%. Under an AEA content of 10%, the compressive strength in comparison with specimens blended with 0 and 5% AEA reduces by 35.3% and 17.5%, respectively.

From the top of Figure 5, the compressive strength of the specimen blended with 1.2 kg/m^3 PPFs is reduced by 13.1% compared to the specimen without fiber. After adding 5% AEA, the decreasing rate of compressive strength is 9.0%. The compressive strength is reduced 2.0% by increasing the content of AEA to 10%.

3.2.2 Splitting tensile strength

It is clear from the bottom of Figure 4 that, as the content of AEA increases from 0 to 5%, the splitting tensile strength of the specimen is reduced by 29.9%. As the content of AEA is increased to 10%, in comparison to specimens mixed with 0 and 5% AEA, the splitting tensile strength is reduced by 52.0% and 31.5%, respectively. When mixing AEA and PPFs in FRAC simultaneously, the decreasing rate of splitting tensile strength is 7.0% when the content of AEA increases from 0 to 5%. When the content of AEA is 10%, the splitting tensile strength is

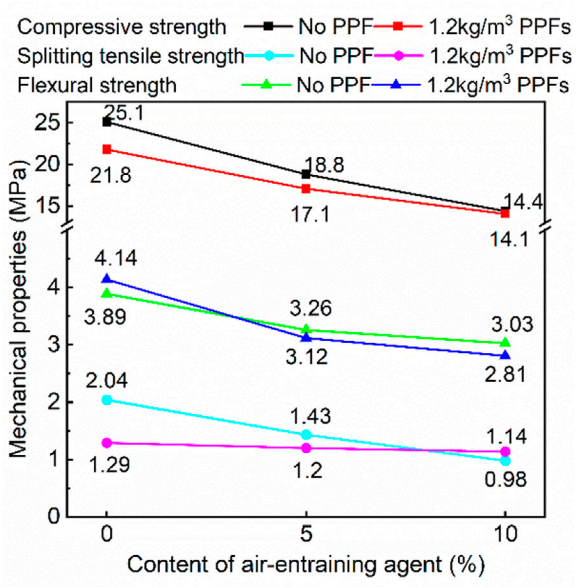

FIGURE 4
Effect of air-entraining agent on mechanical properties.

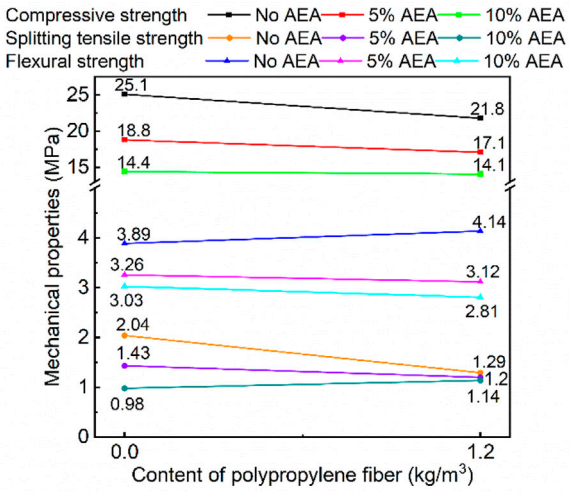

FIGURE 5
Effect of polypropylene fiber on mechanical properties.

decreased by 11.6% and 0.05% in comparison with specimen mixed with 0 and 5% AEA, respectively.

As can be observed from the bottom of Figure 5, the change of splitting tensile strength of specimens with PPFs increments is complicated; it is affected greatly by the content of AEA. The splitting tensile strength of a specimen blended with only PPFs is 36.8% lower than one without fiber. After adding 5% AEA, the splitting tensile strength of a specimen mixed with fiber is reduced by 16.1%. The splitting tensile strength of a specimen mixed with PPFs and 10% AEA increases by 16.3% compared with one blended only with 10% AEA.

3.2.3 Flexural strength

As shown in the middle of Figure 4, as the content of AEA increases from 0 to 5%, the flexural strength is reduced by 16.2%. At an AEA of content 10%, the flexural strength compared with specimens mixed with 0 and 5% AEA decreases by 22.1% and 0.07%, respectively. When mixing PPFs and AEA in FRAC together, as the content of AEA increases from 0 to 5%, the flexural strength decreases by 24.6%; when AEA content is 10%, flexural strength is reduced by 32.1% (from 0% AEA) and 0.10% (from 5% AEA).

It is clear from the middle of Figure 5 that the change trend of the flexural strength of specimens with PPFs is exactly opposite to the splitting tensile strength. The flexural strength of a specimen mixed with only PPFs is increased by 6.4% in comparison to that without fiber. With a mix of PPFs and 5% AEA, the flexural strength of a specimen blended with fiber is reduced by 4.3%. The flexural strength of a specimen mixed with PPFs and 10% AEA decreases by 7.3% from that only blended with 10% AEA. The enhancement effect of PPF on the flexural strength of FRAC is better when there is no AEA.

The compressive strength, splitting tensile strength, and flexural strength of FRAC all decrease significantly with an increase in the content of AEA. This is because, when AEA is blended, air will be introduced into the mixing concrete; airtight tiny bubbles then form inside the concrete, making the unit force area smaller when the concrete bears load, thereby reducing its strength. After incorporating PPFs, while the strength of specimen also decreases with an increase of AEA, the reduction in compressive strength and splitting tensile strength of the specimen decreases, whereas the reduction of flexural strength increases.

PPF is ordinarily regarded as a concrete reinforcement material, but studies illustrate that incorporating PPFs has little effect on the strength of concrete (Bidabadi et al., 2020) or even a negative effect (Haddad et al., 2008). The properties of PPFs are considered to be the main reason for the different effects on the mechanical properties of concrete. The addition of PPFs with low content, with a volume rate of 0.077%–0.2%, leads to an increase in the consistency of fresh concrete, which becomes more pronounced with the increase of fiber admixture, thus affecting the strength of the hardened concrete (Wang et al., 2011). Furthermore, due to the hydrophobicity of PPFs, water is restricted from entering the internal matrix of the concrete and many air bubbles are trapped on the surface of the fiber, causing local softening and the formation of weak areas (Hannawi et al.,

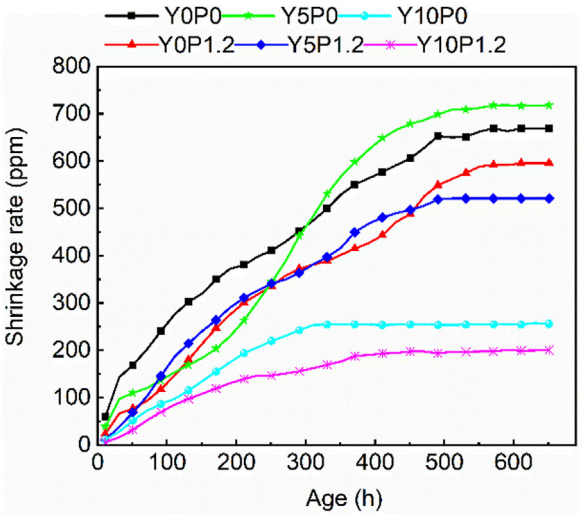

FIGURE 6
Development curve of autogenous shrinkage rate with age.

2016; Gong et al., 2022)—thereby reducing the workability of FRAC.

3.3 Autogenous shrinkage

In this paper, the autogenous shrinkage rate is used to evaluate the autogenous shrinkage of FRAC, as calculated by Eq. 1:

$$\varepsilon_{st} = \frac{(L_{l0} - L_{lt}) - (L_{r0} - L_{rt})}{L_0} \quad (1)$$

where the magnitude of ε_{st} is ppm, being one millionth. L_0 is the initial distance between two reflectors, being 450 mm in the test. L_{l0} and L_{r0} are initial readings of the left and right sensors, respectively. L_{lt} and L_{rt} are readings of the left and right sensors at time t, respectively, and the unit of t is hours.

All other parameters are in millimeters. The development trend of the autogenous shrinkage rate with age is shown in Figure 6.

The autogenous shrinkage rates of FRAC at 3- and 28-day ages measured by the test are listed in Table 4.

As is shown in Figure 6, the autogenous shrinkage rates of the two groups of FRAC with 10% AEA are lower than that of the other groups at all ages. In the case of adding AEA alone, the 3-day autogenous shrinkage rate of FRAC with 10% AEA is reduced by 64.6% and 40.1%, in comparison to that without AEA and that with 5% AEA. The 28-day autogenous shrinkage rate decreased by 60.7% and 63.2%, respectively. The 3- and 28-day autogenous shrinkage rates of FRAC incorporating 10% AEA and PPFs are also much lower than that incorporating 5% AEA and PPFs and that with only PPFs.

At an AEA content of 5%, the early-age autogenous shrinkage rate of FRAC without PPF increased slowly—40.7% lower than that without AEA—while the 28-day autogenous shrinkage rate is the highest among the six groups—6.3% higher than the FRAC without AEA. After adding PPFs with AEA, the autogenous shrinkage rate of the concrete developed steadily; the early-age autogenous shrinkage rates are similar to those of FRAC incorporating only AEA, but the autogenous shrinkage rate at 28-days decreases by 13.9%. Therefore, it is evident that a 10% content of AEA can effectively inhibit the autogenous shrinkage of FRAC, while a 5% content of AEA can inhibit early-age autogenous shrinkage, which promotes the 28-day autogenous shrinkage.

The addition of PPFs can further reduce autogenous shrinkage, and greatly ameliorate the adverse effect of the 5% content of AEA on the 28-day autogenous shrinkage of FRAC. The study showed that the pore structure greatly affects the autogenous shrinkage of concrete; pores with diameters of 5–50 nm will generate significant stresses when drying. The more pores with diameters of 5–50 nm, the more obvious the capillary effect will be, leading to increased autogenous shrinkage (Li et al., 2010; Li and Li, 2014). Therefore, a 5–50 nm pore volumetric percentage is considered the main factor affecting the autogenous shrinkage of concrete. In this experiment, different contents of AEA have outstanding inhibitory effects on the early-age autogenous shrinkage of FRAC, since the AEA introduces a large number of air bubbles with diameters far exceeding 50 nm in the progress of mixing concrete; this thus reduces the volumetric percentage of 5–50 nm pores. In addition, the large number of air bubbles introduced by the addition of high contents of AEA is beneficial in increasing the volume of the cement paste (Piasta and Sikora, 2015), thus compensating for some of the autogenous shrinkage of FRAC. Therefore, the autogenous shrinkage of FRAC mixed with AEA was reduced by different degrees.

In terms of the development trend of the autogenous shrinkage rate of FRAC, the rate before 300 h increased rapidly; after 300 h, the autogenous shrinkage rate of FRAC with 10% AEA added slowed and gradually became stable. The time to stabilization of the autogenous shrinkage rate of FRAC with 5% AEA is around 500 h, while the time for the rate of FRAC without AEA to stabilize is a little longer, around 550 h. Thus, the incorporation of AEA significantly shortens the time for the autogenous shrinkage of FRAC to reach stability.

In the meantime, PPFs can reduce the full-age autogenous shrinkage of FRAC. Without the addition of AEA, the 3-day autogenous shrinkage rate of FRAC with PPFs is reduced by 52.9% and the 28-day rate is decreased by 10.1% compared to FRAC without fiber. The 3- and 28-day autogenous shrinkage rates of FRAC added with PPFs are reduced by 14.8% and 27.8%, respectively, with the addition of 5% both AEA and PPFs. When the content of AEA is increased from 5% to 10%, the 3-day autogenous shrinkage rate of FRAC mixed with PPFs decreased

TABLE 4 Autogenous shrinkage rate at 3 d and 28 d

Specimen ID	Y0P0	Y0P1.2	Y5P0	Y5P1.2	Y10P0	Y10P1.2
Shrinkage rate of 3 d	206	97	122	104	73	54
Shrinkage rate of 28 d	675	604	720	520	265	203

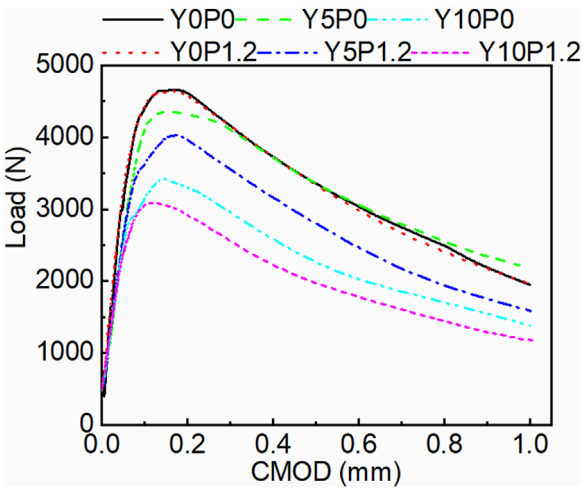

FIGURE 7
P-CMOD curve.

by 26.0% and the 28-day rate decreased by 23.4%. PPFs connect capillary pores to pores in the micron and lower levels, improving the pore structure inside the concrete, and reducing capillary stress and small cracks in the matrix of concrete. At the same time, the addition of PPFs forms a three-dimensional fiber-matrix system inside the concrete and a water film on the surface of the PPFs, both of which limit the loss and migration of water (Wang et al., 2021) and thereby reduce autogenous shrinkage. Furthermore, incorporating PPFs would cause the expansion of mortar in the main peak period of early hydration reaction (Kaufmann et al., 2004), thus compensating for the early-age autogenous shrinkage of FRAC.

3.4 Fracture properties

3.4.1 P-CMOD curve

The values of load and crack-mouth opening displacement of the notched concrete prisms can be obtained and described by the load–crack-mouth opening displacement (P-CMOD) curve, as shown in Figure 7. According to the characteristics of this curve, the failure process of the prism can be divided into three stages. The first is the elastic stage, where the load and crack-mouth opening displacement are in a linear relationship, with the load increasing as the crack mouth opening displacement increases. The slope of the curve, which is the stiffness of the concrete prism (dP/dCMOD), remains basically unchanged. When the stress at the tip of the cut reaches the cracking strength of the concrete, the concrete prism cracks and the elastic stage ends. Following this are two stages of crack propagation. In the first stage, the relationship between load and crack-mouth opening displacement is transformed from the previous linear relationship into a nonlinear relationship. The stiffness of the specimen prism decreases gradually, but the load still increases with the crack-mouth opening displacement until the load increases to its maximum. The typical characteristic of the second stage of crack propagation is that the stiffness value changes from positive to negative, the value of the load begins to decrease, and the crack-mouth opening displacement continues to expand.

The concrete prism changes from the elastic stage to the first stage of crack propagation, which illustrates that the relationship of load and crack-mouth opening displacement transforms from linear to nonlinear. The turning point is the initial crack point, which means that the concrete prism starts to crack at this moment. When the first stage of crack propagation changes to its second stage, the stiffness value changes from positive to negative, indicating that the concrete prism cannot continue to withstand the continued increase in load. The load corresponding to the point where the stiffness is zero represents the critical load of the concrete prism (Zhang and Liu, 2005). After this point, the concrete prism is damaged, and the bearing capacity drops rapidly. In the test, as the load continues to increase, the main crack usually emerges from the incision and then spreads from bottom to top along the mid-span of the prism. After the prism reaches peak load, the main crack extends to the upper third of the prism. The maximum width of the crack is about 0.2 mm, and there will be several tiny cracks beside the main crack, with similar cracks appearing at the same position on the back of the concrete prism.

3.4.2 Fracture toughness

According to Chinese standard DL/T 5332-2005 (National Development and Reform Commission of the People's Republic of China, 2005), there is a transition point from a linear to a non-linear segment in the rising phase of the P-CMOD curve. The load at this transition point is called

TABLE 5 Double-K fracture parameters.

Specimen ID	Initial crack load/N	Critical load/N	a_c/mm	K_{IC}^{ini}/MPa · $\sqrt{m}$	K_{IC}^{un}/MPa · $\sqrt{m}$	K_{IC}^{ini}/K_{IC}^{un}
Y0P0	4065	4657.8	33.7	0.453	0.763	0.594
Y0P1.2	4029.2	4642.8	38.1	0.449	0.826	0.544
Y5P0	3879	4354.2	30.9	0.432	0.770	0.561
Y5P1.2	3349.8	4038	34.7	0.373	0.658	0.567
Y10P0	2834.4	3419.4	36.2	0.316	0.578	0.547
Y10P1.2	2384.8	3085.8	34.6	0.266	0.502	0.529

the initial crack load. Using the line function plug-in Tangent in Origin, we can obtain the value of the initial crack load from the image; the critical load can be obtained according to the three-point bending test. The initial crack load and the critical load are listed in Table 5.

The initial fracture toughness K_{IC}^{ini} of concrete is the boundary value of the stress intensity factor K_I when the crack at the incision of the concrete prism expands, which indicates the ability of concrete to resist crack propagation. The calculation formula of the initial fracture toughness is as follows (Zhou et al., 2022):

$$K_{IC}^{ini} = \frac{3P_{ini}S^{*}10^{-3}}{2h^2B}\sqrt{a_0}f_1\left(\frac{a_0}{h}\right) \tag{2}$$

$$f_1\left(\frac{a_0}{h}\right) = \frac{1.99 - \frac{a_0}{h}\left(1 - \frac{a_0}{h}\right)\left[2.15 - 3.93\frac{a_0}{h} + 2.7\left(\frac{a_0}{h}\right)^2\right]}{\left(1 + 2\frac{a_0}{h}\right)\left(1 - \frac{a_0}{h}\right)^{3/2}} \tag{3}$$

The unstable fracture toughness K_{IC}^{un} of concrete represents the resistance of concrete to forces under critical instability. K_{IC}^{un} can be calculated by the following formula of linear elastic fracture mechanics.

$$K_{IC}^{un} = \frac{3P_{\max}S^{*}10^{-3}}{2h^2B}\sqrt{a_c}f_2\left(\frac{a_c}{h}\right) \tag{4}$$

$$f_2\left(\frac{a_c}{h}\right) = \frac{1.99 - \frac{a_c}{h}\left(1 - \frac{a_c}{h}\right)\left[2.15 - 3.93\frac{a_c}{h} + 2.7\left(\frac{a_c}{h}\right)^2\right]}{\left(1 + 2\frac{a_c}{h}\right)\left(1 - \frac{a_c}{h}\right)^{3/2}} \tag{5}$$

$$a_c = \frac{2}{\pi}h\arctan\sqrt{\frac{BECMOD_c}{32.6P_{\max}} - 0.1135} \tag{6}$$

$$E = \frac{24a_0P_i}{CMOD_iBh}f_3\left(\frac{a_0}{h}\right) \tag{7}$$

$$f_3\left(\frac{a_0}{h}\right) = 0.76 - 2.28\frac{a_0}{h} + 3.87\left(\frac{a_0}{h}\right)^2 - 2.04\left(\frac{a_0}{h}\right)^3 + \frac{0.66}{(1 - a_0/h)^2} \tag{8}$$

In the test, S = 0.3 m, B = 0.1 m, h = 0.1 m, a_0 = 0.02 m. The value of $P_i/CMOD_i$ can be obtained by calculating and averaging the values of three arbitrary points during the linear rising stage of the P-CMOD curve.

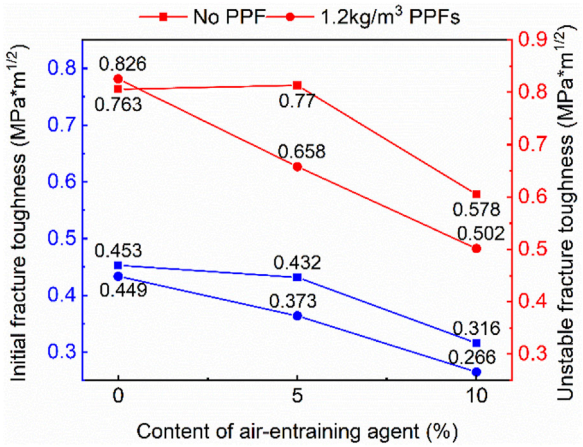

FIGURE 8
Effect of air-entraining agent on initial fracture toughness.

According to Table 5, the change of initial fracture toughness and unstable fracture toughness of FRAC with different AEA and PPFs content can be represented as in Figures 8 and 9.

As shown in Figure 8, without the addition of PPF, the initial fracture toughness of specimen with 5% AEA is reduced by 4.6% in comparison to the case without AEA, and the unstable fracture toughness is almost unchanged. At A AEA content of 10%, the initial fracture toughness is reduced by 30.2%, in comparison to the specimen without AEA, and the unstable fracture toughness is reduced by 24.2%. Compared to the specimen with 5% AEA, the initial fracture toughness is reduced by 26.8% and the unstable fracture toughness is decreased by 24.9%. It is clear that the initial fracture toughness decreases to a small extent and unstable fracture toughness is almost unchanged as the AEA content goes from 0 to 5%, whereas both initial fracture and unstable fracture toughness of a specimen have a large decrease when AEA content is increased from 5% to 10%.

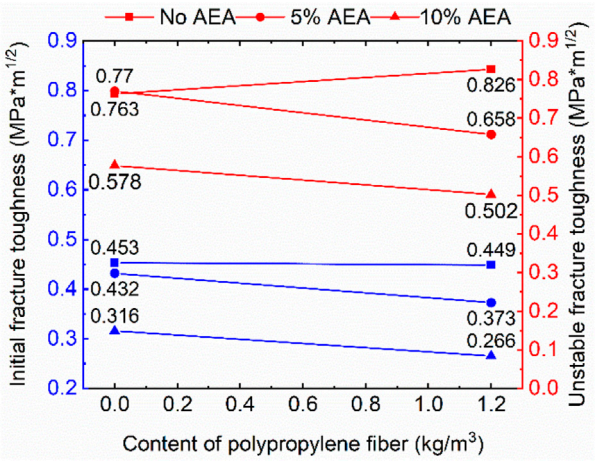

FIGURE 9
Effect of polypropylene fiber on unstable fracture toughness.

After mixing PPFs, the initial fracture toughness of a specimen mixed with 5% AEA is decreased by 16.9% while the unstable fracture toughness is reduced by 20.3%, compared to a specimen without AEA. With AEA content increased to 10%, compared to a specimen without AEA, the initial fracture toughness is reduced 40.8% and the unstable fracture toughness is decreased by 39.2%. In comparison with a specimen with 5% AEA, the initial fracture toughness is reduced by 28.7% and the unstable fracture toughness is reduced by 23.7%. When PPFs and AEA are blended, the initial fracture toughness and unstable fracture toughness of FRAC are significantly reduced with an increase in the content of AEA, and the decrease amplitude is higher than that of no fiber.

From Figure 9, the specimen solely mixed with PPFs has almost no change in initial fracture toughness compared to that without fiber, whereas unstable fracture toughness increases by 7.3%. At an AEA content of 5%, the initial fracture toughness is reduced by 13.7% and the unstable fracture toughness is reduced by 14.5%, in comparison with the specimen with no fiber. With an AEA content of 10%, compared with a specimen without PPF, the initial fracture toughness is reduced 15.8% and the unstable fracture toughness is decreased by 13.1%. The addition of PPFs can slightly improve the fracture properties of FRAC when only PPFs are added. Nevertheless, when adding AEA and PPFs at the same time, the addition of the latter would reduce the fracture properties of FRAC, with the content of AEA blended in concrete having little effect on the reduction amplitude. The effect of PPF on the fracture properties of FRAC is similar to that of the flexural strength. PPFs enhance the fracture properties and flexural strength of plain FRAC. When AEA is added to FRAC, the effect of PPFs on fracture properties and flexural strength changes from increased to decreased. As just PPFs are added to FRAC, before the fracture failure, the main roles of PPFs are to connect the tiny cracks inside FRAC and bear part of the tensile stress (Zhou et al., 2022). Therefore, the initial fracture toughness of FRAC with PPFs and plain FRAC is relatively close, while the unstable fracture toughness of FRAC with PPFs is increased. When PPFs and AEA are simultaneously incorporated into FRAC, a large number of bubbles are introduced into the matrix. Due to the hydrophobicity of PPFs, they will draw bubbles, resulting in many bubbles in the interfacial transition zone (ITZ) around PPFs and forming weak areas (Hannawi et al., 2016). Therefore, the fracture properties and flexural strength of FRAC with PPFs and AEA are lower than those of FRAC with only AEA.

As can be observed from Table 5, the value of K_{IC}^{ini}/K_{IC}^{un} varies between 0.53 and 0.6 in this experiment. The double-K fracture criterion demonstrates that the difference among the values of the initial fracture toughness and the unstable fracture toughness is mainly caused by aggregate. The value of K_{IC}^{ini}/K_{IC}^{un} in this experiment is much higher than the value of ordinary recycled aggregate concrete, which is 0.34 and does not change with recycled aggregate replacement rate (Choubey et al., 2016). This means that, after the specimen prism begins to crack, it takes a shorter time to reach the unstable state and indicates that the resistance of fully recycled aggregate concrete to forces under critical instability is poor.

4 Conclusion

This research has analyzed the effect of air-entraining agent and polypropylene fiber on the density, mechanical properties, autogenous shrinkage properties, and fracture properties of fully recycled aggregate concrete. Its major conclusions are:

1) The incorporation of air-entraining agent reduces the strength and fracture properties of FRAC. As the content of air-entraining agent increases, strength and fracture properties obviously decrease. The incorporation of polypropylene fibers can effectively ameliorate the deterioration effect of the air-entraining agent on compressive strength and splitting tensile strength.
2) The incorporation of 10% air-entraining agent can effectively reduce the full-age autogenous shrinkage of FRAC. The incorporation of 5% air-entraining agent can reduce the 3-day autogenous shrinkage, while increasing 28-day autogenous shrinkage. The incorporation of air-entraining agent can also shorten the time for autogenous shrinkage of FRAC to reach stability. The incorporation of polypropylene fibers can further reduce the autogenous shrinkage of FRAC.
3) The incorporation of only polypropylene fibers will reduce the compressive strength and splitting tensile strength of

concrete, whereas the flexural strength and fracture properties will increase. The incorporation of air-entraining agent can ameliorate the deterioration effect of polypropylene fiber on the compressive strength and splitting tensile strength of FRAC, but flexural strength and fracture properties will change from increased to decreased. Therefore, the improvement effect of polypropylene fiber on the flexural strength and fracture properties of plain FRAC is better than FRAC blended with air-entraining agent.

Data availability statement

The original contributions presented in the study are included in the article/Supplementary Material; further inquiries can be directed to the corresponding author.

Author contributions

DD: methodology, formal analysis, writing. LZ: validation, writing–review and editing, supervision. JZ: review and editing, supervision. CL: investigation and experiments. ZW: investigation, review and editing.

Funding

This research was supported by the National Natural Science Foundation of China (51808509), the Program for Changjiang Scholars and Innovative Research Team in the University of Minister of Education of China (IRT_16R67), and the Henan science and technology research project (212102310402, 202102310281).

Conflict of interest

The authors declare that the research was conducted in the absence of any commercial or financial relationships that could be construed as a potential conflict of interest.

Publisher's note

All claims expressed in this article are solely those of the authors and do not necessarily represent those of their affiliated organizations, or those of the publisher, the editors and the reviewers. Any product that may be evaluated in this article, or claim that may be made by its manufacturer, is not guaranteed or endorsed by the publisher.

References

Ahmed, S. F. U., and Maalej, M. (2009). Tensile strain hardening behaviour of hybrid steel-polyethylene fibre reinforced cementitious composites. *Constr. Build. Mater.* 23 (1), 96–106. doi:10.1016/j.conbuildmat.2008.01.009

Anike, E. E., Saidani, M., Ganjian, E., Tyrer, M., and Olubanwo, A. O. (2019). The potency of recycled aggregate in new concrete: A review. *Constr. Engl.* 19 (4), 594–613. doi:10.1108/ci-07-2018-0056

Bendixen, M., Best, J., Hackney, C., and Iversen, L. L. (2019). Time is running out for sand. *NATURE* 571 (7763), 29–31. doi:10.1038/d41586-019-02042-4

Bidabadi, M. S., Akbari, M., and Panahi, O. (2020). Optimum mix design of recycled concrete based on the fresh and hardened properties of concrete. *J. Build. Eng.* 32, 101483. doi:10.1016/j.jobe.2020.101483

Cakir, O. (2014). Experimental analysis of properties of recycled coarse aggregate (RCA) concrete with mineral additives. *Constr. Build. Mater.* 68, 17–25. doi:10.1016/j.conbuildmat.2014.06.032

Cantero, B., Bravo, M., de Brito, J., Saez del Bosque, I. F., and Medina, C. (2020). Mechanical behaviour of structural concrete with ground recycled concrete cement and mixed recycled aggregate. *J. Clean. Prod.* 275, 122913. doi:10.1016/j.jclepro.2020.122913

Chen, J., Zhao, X., Luo, Y., Deng, X., and Liu, Q. (2014). Investigating freeze-proof durability of C25 shotcrete. *Constr. Build. Mater.* 61, 33–40. doi:10.1016/j.conbuildmat.2014.02.077

China National Standardization Administration CommitteeGeneral Administration of Quality Supervision Inspection and Quarantine of the People's Republic of China (2010). *Recycled coarse aggregate for concrete(GB/T 25177-2010)*. Beijing: China Standard Press. Available at: https://d.wanfangdata.com.cn/standard/ChRTdGFuZGFyZE5ld1MyMDIyMDkwMRIPR0IvVCAyNTE3Ny0yMDEwGgh5enZxMnl4eA%3D%3D.

Cho, B.-S., Han, L. J., and Back, S. (2014). Comparative study on the flexural performance of concrete reinforced with polypropylene and steel fibers. *J. Korean Soc. Civ. Eng.* 34 (6), 1677–1685. doi:10.12652/Ksce.2014.34.6.1677

Choubey, R. K., Kumar, S., and Chakradhara Rao, M. (2016). Modeling of fracture parameters for crack propagation in recycled aggregate concrete. *Constr. Build. Mater.* 106, 168–178. doi:10.1016/j.conbuildmat.2015.12.101

Deng, Z., Liu, X., Yang, X., Liang, N., Yan, R., Chen, P., et al. (2020). A study of tensile and compressive properties of hybrid basalt-polypropylene fiber-reinforced concrete under uniaxial loads. *Struct. Concr.* 22, 396–409. doi:10.1002/suco.202000006

Deresa, S. T., Xu, J., Demartino, C., Heo, Y., Li, Z., and Xiao, Y. (2020). A review of experimental results on structural performance of reinforced recycled aggregate concrete beams and columns. *Adv. Struct. Eng.* 23 (15), 3351–3369. doi:10.1177/1369433220934564

Evangelista, L., and De Brito, J. (2014). Concrete with fine recycled aggregates: A review. *Eur. J. Environ. Civ. Eng.* 18 (2), 129–172. doi:10.1080/19648189.2013.851038

Gao, D., Zhang, L., and Nokken, M. (2017). Mechanical behavior of recycled coarse aggregate concrete reinforced with steel fibers under direct shear. *Cem. Concr. Compos.* 79, 1–8. doi:10.1016/j.cemconcomp.2017.01.006

Gong, J., Ma, Y., Fu, J., Hu, J., Ouyang, X., Zhang, Z., et al. (2022). Utilization of fibers in ultra-high performance concrete: A review. *Compos. Part B Eng.* 241, 109995. doi:10.1016/j.compositesb.2022.109995

Gonzalez, D. C., Mena, A., Minguez, J., and Vicente, M. A. (2021). Influence of air-entraining agent and freeze-thaw action on pore structure in high-strength concrete by using CT-Scan technology. *Cold Regions Sci. Technol.* 192, 103397. doi:10.1016/j.coldregions.2021.103397

Guo, H., Shi, C., Guan, X., Zhu, J., Ding, Y., Ling, T.-C., et al. (2018). Durability of recycled aggregate concrete - a review. *Cem. Concr. Compos.* 89, 251–259. doi:10.1016/j.cemconcomp.2018.03.008

Haddad, R. H., Ai-Saleh, R. J., and Al-Akhras, N. M. (2008). Effect of elevated temperature on bond between steel reinforcement and fiber reinforced concrete. *Fire Saf. J.* 43 (5), 334–343. doi:10.1016/j.firesaf.2007.11.002

Hannawi, K., Bian, H., Prince-Agbodjan, W., and Raghavan, B. (2016). Effect of different types of fibers on the microstructure and the mechanical behavior of Ultra-High Performance Fiber-Reinforced Concretes. *Compos. Part B Eng.* 86, 214–220. doi:10.1016/j.compositesb.2015.09.059

Hua, C., Acker, P., and Ehrlacher, A. (1995). Analyses and models of the autogenous shrinkage of hardening cement paste. *Cem. Concr. Res.* 25 (7), 1457–1468. doi:10.1016/0008-8846(95)00140-8

Kaufmann, J., Winnefeld, F., and Hesselbarth, D. (2004). Effect of the addition of ultrafine cement and short fiber reinforcement on shrinkage, rheological and mechanical properties of Portland cement pastes. *Cem. Concr. Compos.* 26 (5), 541–549. doi:10.1016/s0958-9465(03)00070-2

Khaliq, W., and Waheed, F. (2017). Mechanical response and spalling sensitivity of air entrained high-strength concrete at elevated temperatures. *Constr. Build. Mater.* 150, 747–757. doi:10.1016/j.conbuildmat.2017.06.039

Li, J. J., Niu, J. G., Wan, C. J., Jin, B., and Yin, Y. L. (2016). Investigation on mechanical properties and microstructure of high performance polypropylene fiber reinforced lightweight aggregate concrete. *Constr. Build. Mater.* 118, 27–35. doi:10.1016/j.conbuildmat.2016.04.116

Li, Y., Bao, J., and Guo, Y. (2010). The relationship between autogenous shrinkage and pore structure of cement paste with mineral admixtures. *Constr. Build. Mater.* 24 (10), 1855–1860. doi:10.1016/j.conbuildmat.2010.04.018

Li, Y., and Li, J. (2014). Capillary tension theory for prediction of early autogenous shrinkage of self-consolidating concrete. *Constr. Build. Mater.* 53, 511–516. doi:10.1016/j.conbuildmat.2013.12.010

Liang, N., Ren, L., Tian, S., Liu, X., Zhong, Z., Deng, Z., et al. (2021). Study on the fracture toughness of polypropylene-basalt fiber-reinforced concrete. *Int. J. Concr. Struct. Mat.* 15 (1), 35. doi:10.1186/s40069-021-00472-x

Liu, H., Long, H., and Li, X. (2020). Identification of critical factors in construction and demolition waste recycling by the grey-DEMATEL approach: A Chinese perspective. *Environ. Sci. Pollut. Res.* 27 (8), 8507–8525. doi:10.1007/s11356-019-07498-5

Md, B., and Unnikrishnan, S. (2022). Mechanical strength and impact resistance of hybrid fiber reinforced concrete with coconut and polypropylene fibers. *Mater. Today Proc.* 65, 1873–1880. doi:10.1016/j.matpr.2022.05.048

Ministry of Housing and Urban-Rural Development of ChinaGeneral Administration of Quality Supervision Inspection and Quarantine of the People 's Republic of China (2009). *Standard for test methods of long-term performance and durability of ordinary concrete(GB/T 50082-2009)*. Beijing: China building industry press. Available at: https://d.wanfangdata.com.cn/standard/ChxTdGFuZGFyZE5ld1MyMDIwMDkxODIwMjIwNTMwEg9HQi9UIDUwMDgyLTIwMDkaCGtmdHd1bmxs.

Ministry of Housing and Urban-Rural Development of the People's Republic of ChinaState Administration for Market Regulation (2019). *Standard for test methods of concrete physical and mechanical properties(GB/T 50081-2019)*. Beijing: China Construction Industry Press. Available at: https://d.wanfangdata.com.cn/standard/ChxTdGFuZGFyZE5ld1MyMDIwMDkxODIwMjIwNTMwEg9HQi9UIDUwMDgxLTIwMTkaCDZ1dWM0azZ1.

National Development and Reform Commission of the People 's Republic of China (2005). *Norm for fracture test of hydraulic concrete(DL/T 5332-2005)*. Beijing: China Electric Power Press. Available at: https://d.wanfangdata.com.cn/standard/ChxTdGFuZGFyZE5ld1MyMDIwMDkxODIwMjIwNTMwEg5ETC9UIDUzMzItMjAwNRoIOHdkdGF6eDQ%3D.

National Standardization Management CommitteeState Administration of Market Supervision and Administration (2022). *Sand for construction(GB/T 14684-2022)*. Beijing: China Standard Press. Available at: https://d.wanfangdata.com.cn/standard/ChRTdGFuZGFyZE5ld1MyMDIyMDkwMRIPR0IvVCAxNDY4NC0yMDIyGgg1aHpoaW5hOQ%3D%3D.

Orouji, M., Zahrai, S. M., and Najaf, E. (2021). Effect of glass powder & polypropylene fibers on compressive and flexural strengths, toughness and ductility of concrete: An environmental approach. *Structures* 33, 4616–4628. doi:10.1016/j.istruc.2021.07.048

Piasta, W., and Sikora, H. (2015). Effect of air entrainment on shrinkage of blended cements concretes. *Constr. Build. Mater.* 99, 298–307. doi:10.1016/j.conbuildmat.2015.09.018

Ruan, S., and Unluer, C. (2017). Effect of air entrainment on the performance of reactive MgO and PC mixes. *Constr. Build. Mater.* 142, 221–232. doi:10.1016/j.conbuildmat.2017.03.068

Saje, D., Bandelj, B., Sustersic, J., Lopatic, J., and Saje, F. (2011). Shrinkage of polypropylene fiber-reinforced high-performance concrete. *J. Mat. Civ. Eng.* 23 (7), 941–952. doi:10.1061/(asce)mt.1943-5533.0000258

Shi, C. J., Li, Y. K., Zhang, J. K., Li, W. G., Chong, L. L., and Xie, Z. B. (2016). Performance enhancement of recycled concrete aggregate - a review. *J. Clean. Prod.* 112, 466–472. doi:10.1016/j.jclepro.2015.08.057

Shilang, X., and Reinhardt, H. W. (1999a). Determination of double-K criterion for crack propagation in quasi-brittle fracture, Part I: Experimental investigation of crack propagation. *Int. J. Fract.* 98 (2), 111–149. doi:10.1023/a:1018668929989

Shilang, X., and Reinhardt, H. W. (1999b). Determination of double-K criterion for crack propagation in quasi-brittle fracture. II. Analytical evaluating and practical measuring methods for three-point bending notched beams. *Int. J. Fract.* 98 (2), 151–177. doi:10.1023/A:1018740728458

Tazawa, E., and Miyazawa, S. (1995). EXPERIMENTAL-STUDY on mechanism of autogenous shrinkage of concrete. *Cem. Concr. Res.* 25 (8), 1633–1638. doi:10.1016/0008-8846(95)00159-x

Torres, A., Brandt, J., Lear, K., and Liu, J. (2017). A looming tragedy of the sand commons. *Science* 357 (6355), 970–971. doi:10.1126/science.aao0503

Wang, L., He, T., Zhou, Y., Tang, S., Tan, J., Liu, Z., et al. (2021). The influence of fiber type and length on the cracking resistance, durability and pore structure of face slab concrete. *Constr. Build. Mater.* 282, 122706. doi:10.1016/j.conbuildmat.2021.122706

Wang, L., Li, G., Li, X., Guo, F., Tang, S., Lu, X., et al. (2022a). Influence of reactivity and dosage of MgO expansive agent on shrinkage and crack resistance of face slab concrete. *Cem. Concr. Compos.* 126, 104333. doi:10.1016/j.cemconcomp.2021.104333

Wang, L., Zhou, S., Shi, Y., Huang, Y., Zhao, F., Huo, T., et al. (2022b). The influence of fly ash dosages on the permeability, pore structure and fractal features of face slab concrete. *Fractal Fract.* 6 (9), 476. doi:10.3390/fractalfract6090476

Wang, Q., Cong, P., Yang, H., and Chen, S. (2014). Influence of compounding shrinkage reducing agent and air entraining agent on crack resistance of cement mortar. *Concrete* (1), 117–120. (in Chinese). doi:10.3969/j.issn.1002-3550.2014.01.033

Wang, S., Zhu, X., Wang, W., and Li, J. (2011). "The analysis on how the polypropylene fiber reinforced concrete works," in *Advances in structures*. PTS 1-5, International conference on structures and building materials, Guangzhou, January 07–09, 2011. doi:10.4028/www.scientific.net/AMR.163-167.4580

Wu, Z., Libre, N. A., and Khayat, K. H. (2020). Factors affecting air-entrainment and performance of roller compacted concrete. *Constr. Build. Mater.* 259, 120413. doi:10.1016/j.conbuildmat.2020.120413

Yang, H. M., Zhang, S. M., Wang, L., Chen, P., Shao, D. K., Li, J. Z., et al. (2022). High-ferrite portland cement with slag: Hydration, microstructure, and resistance to sulfate attack at elevated temperature. *Cem. Concr. Compos.* 130, 104560. doi:10.1016/j.cemconcomp.2022.104560

Zhang, H., Wang, Y.-Y., Lehman, D. E., and Geng, Y. (2020). Autogenous-shrinkage model for concrete with coarse and fine recycled aggregate. *Cem. Concr. Compos.* 111, 103600. doi:10.1016/j.cemconcomp.2020.103600

Zhang, H., Xiao, J., Tang, Y., Duan, Z., and Poon, C.-s. (2022). Long-term shrinkage and mechanical properties of fully recycled aggregate concrete: Testing and modelling. *Cem. Concr. Compos.* 130, 104527. doi:10.1016/j.cemconcomp.2022.104527

Zhang, J., and Liu, Q. (2005). "Method for determining fracture mechanical parameters of concrete by three-point bending test," in The 7th Council Meeting and Academic Exchange Conference of Concrete and Cement Products Branch of China Portland Society, Haikou, China, October 17 (HaiKou) (in Chinese).

Zhou, W., Mo, J., Zeng, L., and Xiang, S. (2022). Fracture behavior of polypropylene fiber reinforced concrete modified by rubber powder exposed to elevated temperatures. *Constr. Build. Mater.* 346, 128439. doi:10.1016/j.conbuildmat.2022.128439

Nomenclature

ε_{st} shrinkage rate at test period t(h)

L_{lt} reading of left sensor at t(h)

L_{rt} reading of right sensor at t(h)

a effective crack extension length

a_0 initial crack length

a_c critical effective crack length

S specimen span

B specimen width

h specimen height

E elastic modulus

L_{lo} initial reading of left sensor

L_{ro} initial reading of right sensor

L_0 initial distance between two reflectors

P_{max} critical load

$CMOD$ crack mouth opening displacement

$CMODc$ critical crack mouth opening displacement

K_{IC}^{ini} initial fracture toughness

K_{IC}^{un} unstable fracture toughness

K_I stress intensity factor